INL/CON-17-43689-Revision-0

EFFECT OF DISCRETIZATION ERROR ON THE QUANTIFICATION OF MODEL UNCERTAINTY IN TWO-PHASE FLOW SIMULATIONS

Ling Zou, Tomasz Kozlowski, Guojun Hu

May 2018

The INL is a U.S. Department of Energy National Laboratory
operated by Battelle Energy Alliance

INL/CON-17-43689-Revision-0

EFFECT OF DISCRETIZATION ERROR ON THE QUANTIFICATION OF MODEL UNCERTAINTY IN TWO-PHASE FLOW SIMULATIONS

Ling Zou, Tomasz Kozlowski, Guojun Hu

May 2018

Idaho National Laboratory
Idaho Falls, Idaho 83415

http://www.inl.gov

Prepared for the
U.S. Department of Energy

Under DOE Idaho Operations Office
Contract DE-AC07-05ID14517

EFFECT OF DISCRETIZATION ERROR ON THE QUANTIFICATION OF MODEL UNCERTAINTY IN TWO-PHASE FLOW SIMULATIONS

G. Hu[1], L. Zou[2], and T. Kozlowski[1]
[1] University of Illinois at Urbana-Champaign, Talbot Laboratory, 104 S Wright St, Urbana, IL, 61801, United States
[2] Idaho National Laboratory, 2525 N Freemont Ave., Idaho Falls, ID 83415, United States

ghu3@illinois.edu, Ling.Zou@inl.gov, and txk@illinois.edu

ABSTRACT

Verification, validation and uncertainty quantification (VVUQ) have become a common practice in thermal-hydraulics analysis. In general, these activities deal with propagations of uncertainties in computer code simulations, e.g., through system analysis codes. However, most existing such activities in thermal-hydraulics analysis have been primarily focused on input and model uncertainties, while numerical errors were largely overlooked. Numerical errors can appear in many different forms, e.g., round-off error, statistical sampling error, and discretization error. In thermal-hydraulics analysis, especially two-phase flow simulations commonly encountered in reactor safety analysis, the lack of consideration of discretization error is mainly due to the difficulty in estimating them. Accurate estimations of discretization error require continuous mesh refinement and/or implementation of high-order numerical schemes in system analysis code, both of which are difficult to achieve in existing codes. In this work, we will build a computer code that incorporates both first-order and second-order numerical methods to solve the two-phase flow problems. The first-order method resembles the one used in many existing system analysis codes; and the second-order method works as the reference to estimate numerical errors. Numerical verification of spatial discretization schemes will be presented in the form of mesh convergence study. It will also be demonstrated via case studies that, in practical scenarios, discretization errors can be as large as, or even larger than, model uncertainties.

1. INTRODUCTION

In recent years, verification, validation and uncertainty quantification (VVUQ) have become a common practice in thermal-hydraulics analysis. In general, these activities deal with propagations of uncertainties in computer code simulations, e.g., through system analysis codes. However, most of such activities in thermal-hydraulics analysis have been primarily focused on model uncertainties, while numerical uncertainties were largely overlooked. Numerical uncertainties (or numerical errors) can appear in many different forms, e.g., round-off error, statistical sampling error, and discretization error. As pointed out by Oberkampf and Roy [1], discretization error is usually the largest, however the most difficult type of error to estimate reliably.

In thermal-hydraulics analysis, especially two-phase flow simulations commonly encountered in reactor safety analysis, the lack of consideration of discretization error is mainly due to the difficulty in estimating it. Accurate estimation of discretization error requires continuous mesh refinement and/or implementation of high-order numerical schemes, both of which are unfortunately very difficult to achieve in existing codes. It should be emphasized that mesh refinement (or mesh sensitivity study) is a well-understood concept in the thermal-hydraulics field (see, for example, the discussion in section 3.7.2 of [2]). However, it is not commonly practiced for many reasons, e.g., lack of understanding of numerical error by code users, consideration of computational cost, deteriorated numerical stability with refined meshes, etc. Secondly, high-order (e.g., second-order) numerical schemes are simply unavailable in almost all existing system analysis code. Implementation of high-order numerical schemes in these codes is difficult, if not impossible, given the complexity of these codes.

On the other hand, some in the field tend to argue that numerical uncertainties (or discretization error as we have emphasized) are not as important as the large uncertainties in two-phase flow models, e.g., closure correlations. As a result, nodalization can be manipulated unintentionally, or maybe intentionally, to match experimental data, which is referred to as '*user effects*' or '*compensating errors*[1]' [3] in thermal-hydraulics community. Such a practice is highly criticized by Levy (page 147, [2]).

In this work, first we will build a computer code that incorporates both first-order and second-order numerical method to solve the two-phase flow problems. The first-order method resembles the one used in existing system analysis code (e.g. RELAP5); and the second-order method works as the reference to estimate numerical errors. Next, numerical verification of spatial discretization schemes will be presented in the form of mesh convergence study. Finally, it will be demonstrated via case studies that, in practical scenarios, discretization errors can be as large as, or even larger than, model uncertainties.

2. SOLVER FOR TWO-FLUID TWO-PHASE FLOW MODEL

In this section, a brief introduction will be given to the six-equation two-fluid two-phase flow model. This model is widely used in existing system analysis codes, and thus provides a good basis for numerical error and model uncertainty quantification.

2.1 Flow Model

The two-fluid two-phase flow model used in this paper is the same as used in the RELAP5-3D code [4], which includes a set of mass, momentum, and energy equations for each phase, which are summarized as,

[1] We treat nodalization as one kind of those parameters that can be 'tuned' that cause 'compensating errors' as discussed in reference [3].

$$\frac{\partial(\alpha_l\rho_l)}{\partial t}+\frac{\partial(\alpha_l\rho_l u_l)}{\partial x}=-\Gamma_g \quad (1)$$

$$\frac{\partial(\alpha_g\rho_g)}{\partial t}+\frac{\partial(\alpha_g\rho_g u_g)}{\partial x}=\Gamma_g \quad (2)$$

$$\alpha_l\rho_l\frac{\partial u_l}{\partial t}+\alpha_l\rho_l u_l\frac{\partial u_l}{\partial x}+\alpha_l\frac{\partial p}{\partial x}-\alpha_l\rho_l g_x-F_{int}+F_{wall,l}+\Gamma_g(u_{int}-u_l)=0 \quad (3)$$

$$\alpha_g\rho_g\frac{\partial u_g}{\partial t}+\alpha_g\rho_g u_g\frac{\partial u_g}{\partial x}+\alpha_g\frac{\partial p}{\partial x}-\alpha_g\rho_g g_x+F_{int}+F_{wall,g}-\Gamma_g\left(u_{int}-u_g\right)=0 \quad (4)$$

$$\frac{\partial(\alpha_l\rho_l e_l)}{\partial t}+\frac{\partial(\alpha_l\rho_l u_l e_l)}{\partial x}+p\frac{\partial\alpha_l}{\partial t}+p\frac{\partial(\alpha_l u_l)}{\partial x}-Q_{wl}-Q_{il}+\Gamma_{ig}h_l^*+\Gamma_w h_l'=0 \quad (5)$$

$$\frac{\partial\left(\alpha_g\rho_g e_g\right)}{\partial t}+\frac{\partial\left(\alpha_g\rho_g u_g e_g\right)}{\partial x}+p\frac{\partial\alpha_g}{\partial t}+p\frac{\partial\left(\alpha_g u_g\right)}{\partial x}-Q_{wg}-Q_{ig}-\Gamma_{ig}h_g^*-\Gamma_w h_g'=0 \quad (6)$$

where, subscripts *l* and *g* denote the liquid phase and the gas phase, respectively; and subscript '*int*' denotes interface. Γ_g is net vapor generation rate due to wall boiling/condensation (Γ_w), and bulk evaporation/condensation (Γ_{ig}). $F_{wall,l}$ and $F_{wall,g}$ are wall friction terms. Q_{wl} and Q_{wg} are wall-to-liquid and wall-to-gas phase heat transfer terms, respectively. Q_{il} and Q_{ig} are the interface-to-liquid and interface-to-gas phase heat transfer terms, respectively. h_l' and h_g' are phasic enthalpy carried by wall vapour generation term. h_l^* and h_g^* are phasic enthalpy carried by interfacial mass transfer term.

2.2 Closure Correlations

The equation system is augmented with closure models that predict local two-phase flow regimes, wall heat transfer, wall boiling, interfacial heat/mass transfer, and interfacial momentum exchange. In this paper, flow regime is considered for vertical flow under pre-CHF (critical heat flux) conditions only, which include single-phase liquid, bubbly, slug, annular mist, and mist flow regimes. Wall heat transfer is considered for single-phase flow and nucleate boiling conditions. Wall friction is considered for both single-phase flow and two-phase flow conditions. For two-phase wall friction, two-phase multiplier concept is used. Interfacial heat, mass, and momentum exchanges are treated in all two-phase flow regimes mentioned above. Most of the closure correlations are taken from the RELAP5-3D code [4]. Table 1 gives a brief summary of closure correlations types and references.

Table 1 - Closure correlations implemented in this work

Closure correlation	Model and references
Flow regime map	RELAP5-3D [4]
Subcooled boiling	Saha-Zuber; Lahey model [4]
Interfacial drag	EPRI drift flux model [4, 5]
Interfacial heat transfer	RELAP5-3D [4]
Wall friction	Two-phase multiplier [4]

2.3 Numerical Methods

A computer code has been developed to incorporate both first-order and second-order numerical schemes. First-order scheme is based on a first-order fully implicit Backward Euler (BDF1) time integration scheme and a first-order upwind spatial discretization scheme with staggered grid.

Such first-order numerical scheme resembles those used in many existing system analysis codes, e.g., RELAP5 [4]. Second-order scheme is based on the fully implicit BDF2 time integration scheme and a second-order upwind scheme with staggered grid. The fundamental concept of the second-order upwind scheme is similar to the first-order one, however higher spatial accuracy is achieved via linear reconstruction of local variables. In a previous work, we have demonstrated its second-order accuracy, but only with a simplified two-phase problem that has analytical solution [6]. These methods have also been successfully applied to solve more complicated two-phase flow problems [7]. To resolve the non-linearity of the two-phase flow equation system, a Jacobian-free Newton-Krylov (JFNK) method is employed. For brevity, details of numerical schemes and the implementation of JFNK method are omitted in this paper, both of which have been thoroughly discussed in our previous papers [6, 7].

2.4 Mesh Convergence Study

Rigorous mesh convergence studies are very rare for most existing system analysis codes. The reasons are complicated, for example, deteriorated numerical stability, discontinuities in closure correlations, concerns about the validity of closure correlations as meshes are continuously refined, etc. On the contrary, superior numerical stability has been observed for the computer code developed and used in this paper. The reason for such stable behaviour is not fully understood, we attribute it to the fully implicit method that fully resolves the non-linearity of the equation system.

Table 2 - Test conditions of the FRIGG 413-125 test

Parameter	Value
Channel type	Rod bundle
Channel length	4.365 m
Pressure	7.0 MPa
Inlet subcooling	15.3 K
Inlet mass flux	950 kg/m^2-s
Wall heat flux	664 kW/m^2
Outlet void fraction	~0.75

In this paper, mesh convergence study is performed on a realistic two-phase flow problem, namely the FRIGG 413-125 test [8]. The test loop consisted of 36 rods with 4.365 m uniformly heated length and 13.8 mm outer diameter. An additional unheated rod with 20 mm outer diameter was present in the center of the rod bundle. All rods were housed in a cylinder shroud, with 159.5 mm inner diameter. Table 2 lists the test conditions for this test.

For mesh convergence study, ideally, analytical solution or manufactured solution should be used as the reference solution. However, analytical solutions rarely exist for realistic two-phase flow problems, and we have to rely on numerical results using very fine meshes and high-order numerical schemes. In this case, numerical results using 640 finite volume cells with second-order accuracy are used as the reference solution. Figure 1 shows results for mesh convergence of void fraction using the L-1 error norm. Number of finite volume cells is continuously refined by a factor of 2 from 5 to 320. It is noted that the L-1 error norm of void fraction has important physical meaning, it is an error estimation of total driving force in two-phase natural circulation loop. We see in Figure 1 that we obtain expected order of accuracy, i.e. 1.02 for the first-order

scheme and 1.89 for the second-order scheme. Moreover, the second-order method results in orders of magnitude lower error compared to its first-order counterpart. For a practical mesh size, e.g. 40 cells, the numerical error of the second-order scheme is ~100 times less than that of the first-order scheme. The practical impact of numerical errors is demonstrated in Figure 2, which shows numerical results from both spatial schemes with different mesh sizes. As shown in Figure 2, almost all numerical results that use the second-order spatial scheme nicely collapse on a single line. On the contrary, numerical results that use the first-order spatial scheme scatter significantly. For the case with 5 finite volume cells, numerical uncertainty due to discretization error can be as large as 0.2 in void fraction prediction. Comparison between these two figures clearly demonstrates the advantage of using second-order schemes in system analysis codes, e.g., nodalization (user) effect is greatly reduced.

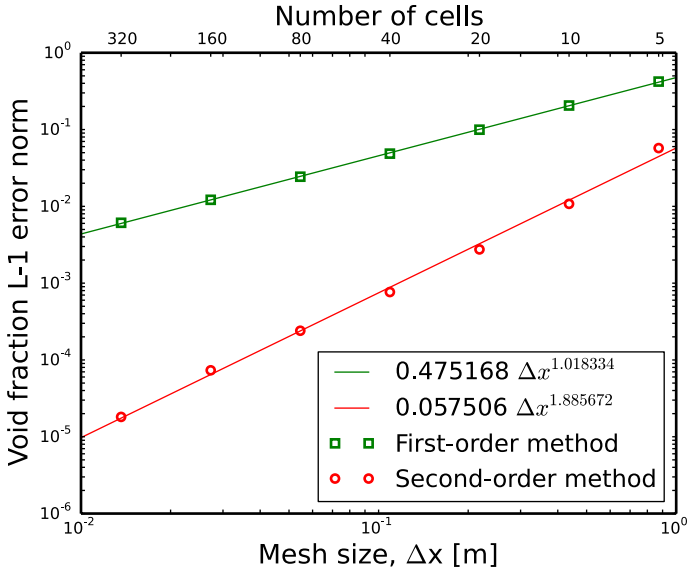

Figure 1 - Mesh convergence study for FRIGG 413-125 test.

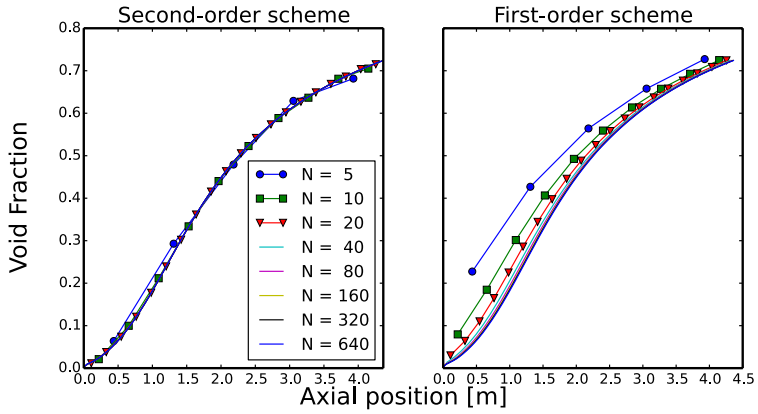

Figure 2 - Numerical results on void fraction using second-order (left) and first-order (right) spatial schemes.

3. DISCRETIZATION ERROR VS MODEL UNCERTAINTY

Figure 3 shows schematic of model uncertainty quantification and discretization error quantification. In Figure 3, ME_C and ME_F represent the model uncertainty in code prediction with a coarse mesh (C) and a fine mesh (F); ME_R represents the real uncertainty; BE_C and BE_F represent the bias in code prediction with a coarse mesh and a fine mesh; DE represents the discretization error of code prediction with a coarse mesh. Ideally, the BE_F error should be minimized in a simulation; however, nodalization can be tuned, sometimes unintentionally, sometimes intentionally, to minimize the BE_C error in thermal-hydraulics solution. Ideally, the ME_F should be studied to quantify the model uncertainty; however, it is ME_C that is most commonly studied in thermal-hydraulics community. Our main concern is the reliability of the model uncertainty (ME_C), which is obtained with a coarse mesh (and a low-order solver). Note that the measurement data to quantify ME_R is usually not available. In this work, we will focus on quantifying the model uncertainty (with coarse and fine mesh) and the discretization error.

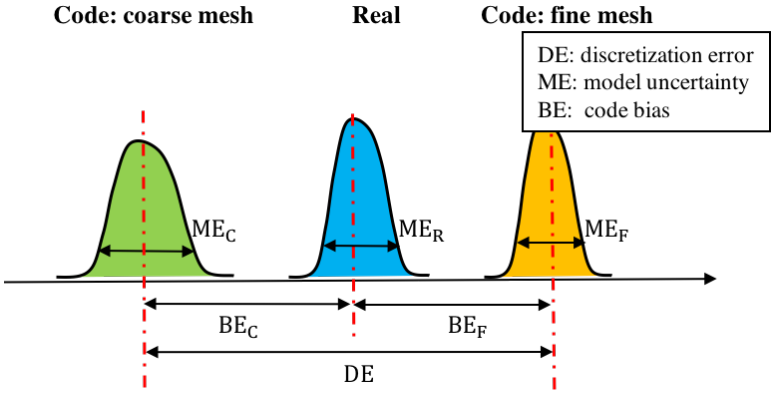

Figure 3 - Schematic of discretization error and model uncertainty

Bartolomei [9] subcooled flow boiling test case is used to quantify the discretization error and model uncertainty in the void fraction. Conditions of the Bartolomei subcooled flow boiling test are summarized in Table 3. Discretization error and model uncertainty in void fraction will be quantified at three positions, i.e. P1 (1.0 m), P2 (1.2 m), and P3 (1.4 m).

Table 3 - Test conditions of the Bartolomei test

Parameter	Value
Channel type	Round tube
Channel length	1.5 m
Pressure	6.84 MPa
Inlet subcooling	91.55 K
Inlet mass flux	961 kg/m^2-s
Wall heat flux	1.13 MW/m^2
Outlet void fraction	~0.6

3.1 Parameters of Interest

The uncertainty in the void fraction prediction comes from many sources, e.g. uncertainty in the closure correlations and uncertainty in the boundary conditions. In this paper, we treat the uncertainties due to the boundary conditions and closure correlations similarly. And, for the

purposes of this paper we call them the model uncertainty. The model uncertainty due to the boundary conditions is studied by applying the coefficients ω to the boundary conditions, i.e.

$$\begin{aligned} p_{outlet} &\leftarrow \omega_{P_o} p_{outlet} \\ \mathrm{Mass}_{inlet} &\leftarrow \omega_{mass} \mathrm{Mass}_{inlet} \\ q_{wall} &\leftarrow \omega_{Q_w} q_{wall} \\ T_{l,inlet} &\leftarrow T_{l,inlet} + \omega_{T_l} \end{aligned} \tag{7}$$

The model uncertainty due to the closure correlations is studied by applying the coefficients ω to the closure correlations, i.e.

$$\begin{aligned} F_{int} &\leftarrow \omega_{F_i} F_{int} \\ F_{wall,l} &\leftarrow \omega_{F_{wl}} F_{wall,l} \\ F_{wall,g} &\leftarrow \omega_{F_{wg}} F_{wall,g} \\ H_{il} &\leftarrow \omega_{H_{il}} H_{il} \\ H_{ig} &\leftarrow \omega_{H_{ig}} H_{ig} \end{aligned} \tag{8}$$

For the selected Bartolomei case, where the inlet subcooling is high, the subcooled boiling model has large impact on the predicted void fraction. Thus, another coefficient, $\omega_{h_{cr}}$, is used to modify the subcooled boiling model, i.e.

$$\begin{aligned} h_{cr} &= h_{l,sat} - \frac{\mathrm{St}\, C_{pl}}{\omega_{h_{cr}} \mathrm{St}_{cr}}, \text{for } \mathrm{Pe} < 70000 \\ h_{cr} &= h_{l,sat} - \frac{\mathrm{Nu}\, C_{pl}}{\omega_{h_{cr}} \mathrm{Nu}_{cr}}, \text{for } \mathrm{Pe} \geq 70000 \end{aligned} \tag{9}$$

For most of the parameters of interest, the uncertainty information (or more importantly the probability distribution) is unavailable. The common practice is to use an ad-hoc distribution that is based on expert judgements. Another promising method is the so-called inverse uncertainty quantification method [[12], 13], which quantifies the physical model uncertainty based on experiment data and code prediction. Either way, we need to specify the distribution of parameters ω prior to the model uncertainty quantification. Based on experimental data in [[10]], a ±25% error bar was given to the fitted correlation, which is used as the bound for the distribution in simulations to estimate its impact on numerical results. In this work, the probability distribution for the parameters ω are listed in Table 4. The standard deviation for the boundary condition parameters is taken from [[11]]. The standard deviation for the closure correlations parameters is set at 0.1, which is an ad-hoc choice. This choice ensure that most samples are within 25% of the nominal value. For the selected test case, where the inlet subcooling is high, Saha-Zuber correlation [[10]], which determines the conditions necessary for net void to exist, has been found to have a large impact on void fraction prediction. Two additional justifications for this ad-hoc normal distribution are: 1) in this work, we are mainly interested in the effect of the discretization error on the model uncertainty, not the model uncertainty itself; 2) the behaviour of the output (i.e. void fraction) is approximately a linear function (see Figure 4) of the input coefficients ω, which means the shape (e.g. normal, log-normal, etc.) of the distribution is less important. Figure 4 also shows that the void fraction is not

sensitive to the wall-to-gas friction and interface-to-gas heat transfer coefficient, thus, we will not consider these two coefficients in the following discussion.

Table 4 - Probability distribution of boundary condition and closure correlation parameters

Parameter	Parameter name	PDF	Mean	Stand. Dev.
ω_{P_o}	Outlet pressure	Normal	1.0	1%
ω_{mass}	Inlet mass flux	Normal	1.0	1%
ω_{Q_w}	Wall heat flux	Normal	1.0	1.5%
ω_{T_l}	Inlet water temperature	Normal	0.0	1.0 K
$\omega_{h_{cr}}$	Critical enthalpy (Saha-Zuber model)	Normal	1.0	10%
ω_{F_i}	Interfacial friction	Normal	1.0	10%
$\omega_{F_{wl}}$	Wall-to-liquid friction	Normal	1.0	10%
$\omega_{F_{wg}}$	Wall-to-gas friction	Normal	1.0	10%
$\omega_{H_{il}}$	Interface-to-liquid heat transfer coefficient	Normal	1.0	10%
$\omega_{H_{ig}}$	Interface-to-gas heat transfer coefficient	Normal	1.0	10%

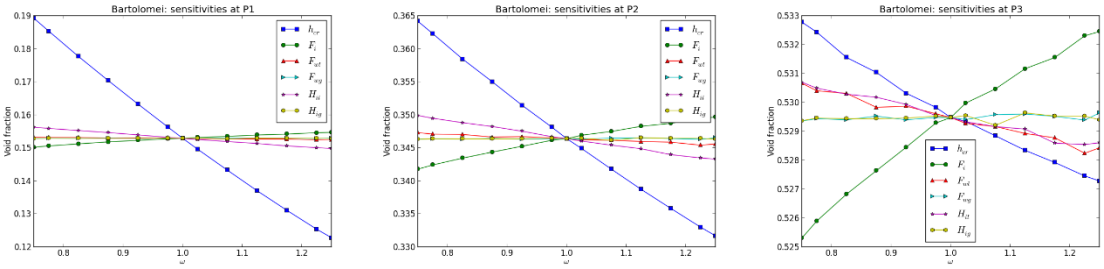

Figure 4 - Behaviour of void fraction for different closure correlation parameters at 3 different positions. Results are obtained with the second-order scheme and 80 cells

3.2 Quantification of Discretization Error and Model Uncertainty

Given the probability distribution of the physical models (or closure correlations), the model uncertainty could be obtained by performing an uncertainty quantification analysis; the discretization error could be obtained by a mesh convergence study. A series of simulations are performed to quantify the discretization error and model uncertainty. The discretization error is quantified by simulating the selected Bartolomei problem with 20, 40, and 80 uniform cells using both the first-order and the second-order solver. The results obtained with 80 cells second-order solver are used as the base (reference solution) to quantify the discretization error. For each mesh size, 800 samples of each boundary condition and physical model parameter are produced according to the distribution given in Table 4. Then, the uncertainty in void fraction is quantified as the standard derivation of the generated void fraction samples.

Figure 5, Figure 6, and Figure 7 shows the discretization error and model uncertainty in the void fraction prediction. Unlike Figure 6 and Figure 7 that show the model uncertainty for a single effect, Figure 5 shows the model uncertainty that account for all source of uncertainties, i.e. the boundary conditions and the closure correlations. Table 5, Table 6, and Table 7 lists quantitatively the discretization error and model uncertainty at three positions. In Figure 5 and Figure 6, the 3σ (or 99.7% confidence level) error bar and the mean value is plotted for two extreme cases, i.e. coarse mesh with first-order solver and fine mesh with second-order solver. From Figure 5 and Figure 6, we see that the discretization error is comparable (even larger) to the model uncertainties. For some closure correlations (e.g. interfacial friction, wall friction, and interfacial heat transfer coefficient), the discretization error is much larger than the model uncertainty. Note that the model uncertainty due to the wall friction and interfacial heat transfer coefficient is omitted here as they are very similar to the model uncertainty due to the interfacial friction. As an example, Figure 7 (and part of Figure 5) show selected distributions of the void fraction due to 4 parameters at three positions. We see that as the mesh is refined, the distribution of the void fraction prediction converges to the reference obtained with a fine mesh with second-order solver. In addition, we see that the discretization has an effect on the distribution of the void fraction, meaning that the model uncertainty might not be reliable when using a coarse mesh with a low-order solver.

4. CONCLUSION

In this paper, rigorous numerical and model uncertainty analyses were performed with a new computer code that solves two-fluid two-phase flow problems using both first-order and second-order numerical schemes. Rigorous numerical verification was performed by mesh convergence study of a FRIGG experiment test case, where expected order of accuracy was achieved for both schemes. Based on the successful implementation of the second-order scheme, a reliable estimation of the discretization error was performed. The Bartolomei subcooled flow boiling test was used to quantify the discretization error and the model uncertainty (including the uncertainty in boundary conditions and closure correlations) through an uncertainty quantification analysis. An sensitivity analysis was at first performed with respect to the boundary conditions and closure correlations. It was found that the behaviour of the output (i.e. void fraction) is approximately a linear function of the interested parameters (e.g. boundary conditions), which means the shape (e.g. normal, log-normal, etc.) of the distribution is less important. It was also found that the void fraction is not sensitive to the wall-to-gas friction and interface-to-gas heat transfer coefficient. Then the discretization error and model uncertainty was quantified using the Bartolome test. It was found that the discretization error is comparable (even larger) to the model uncertainties. For some closure correlations (e.g. interfacial friction, wall friction, and interfacial heat transfer coefficient), the discretization error is much larger than the model uncertainty. These findings clearly demonstrate the advantages of using high-order numerical schemes in system analysis codes.

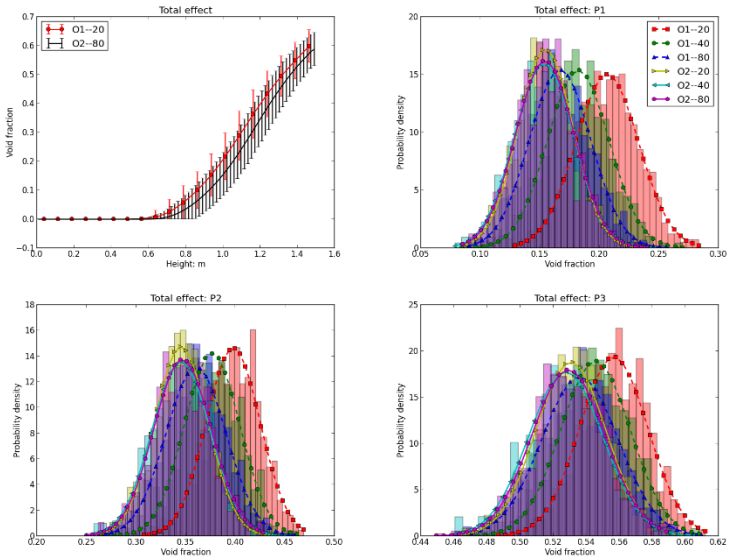

Figure 5 - Discretization error and model uncertainty (total effect) in void fraction

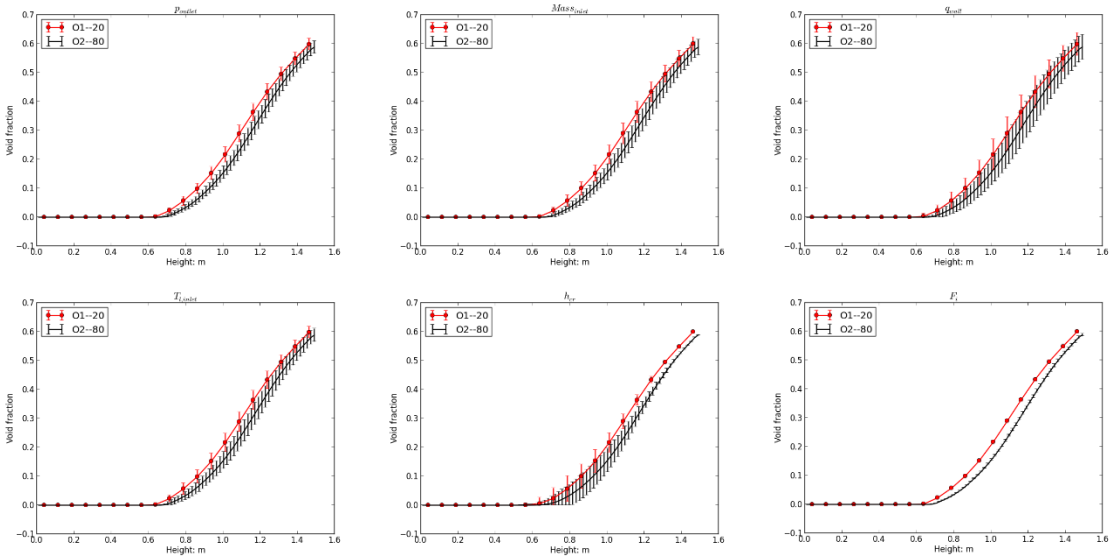

Figure 6 - Discretization error and model uncertainty in void fraction. The error bar represents 99.7% confidence level. Upper row (left: outlet pressure; middle: inlet mass flux; right: wall heat flux). Lower row (left: inlet water temperature; middle: Saha-Zuber model; right: interfacial friction).

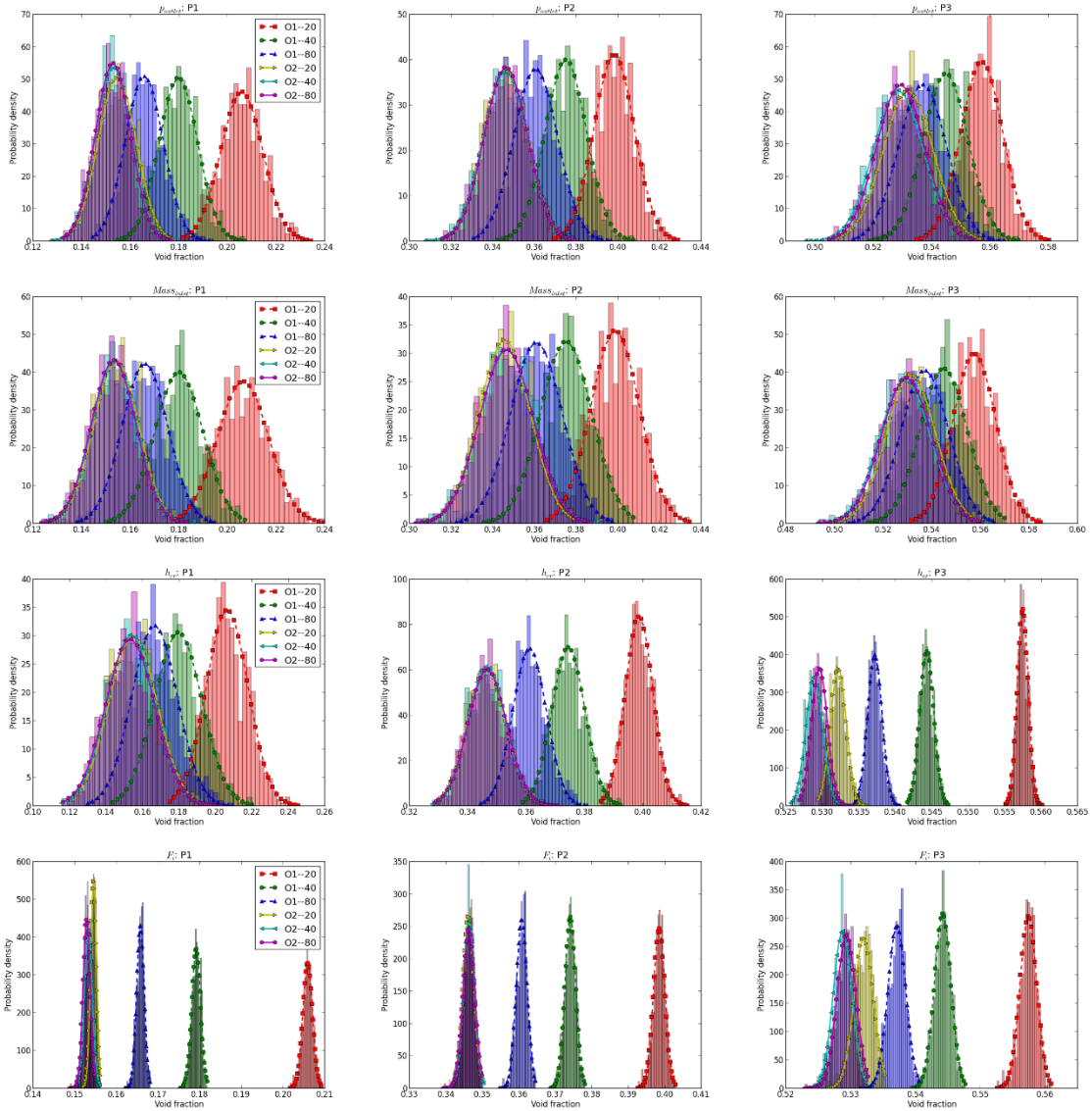

Figure 7 - Discretization error and model uncertainty in void fraction at three positions (left: P1; middle: P2; right: P3). First row: outlet pressure; second row: inlet mass flux; third row: Saha-Zuber model; fourth row: interfacial friction

Table 5 - Discretization error vs model uncertainty in void fraction at 3 positions I: total effect

	P1			P2			P3		
	Mean	DE	ME	Mean	DE	ME	Mean	DE	ME
	Total effect								
1st, 20	0.2054	5.09E-02	2.47E-02	0.3970	5.03E-02	2.55E-02	0.5560	2.69E-02	1.95E-02
1st, 40	0.1779	2.34E-02	2.41E-02	0.3717	2.50E-02	2.70E-02	0.5419	1.29E-02	2.08E-02
1st, 80	0.1655	1.10E-02	2.40E-02	0.3586	1.18E-02	2.70E-02	0.5348	5.74E-03	2.06E-02
2nd, 20	0.1544	1.44E-04	2.29E-02	0.3456	1.10E-03	2.65E-02	0.5313	2.27E-03	2.06E-02
2nd, 40	0.1539	6.59E-04	2.23E-02	0.3447	2.05E-03	2.70E-02	0.5267	2.35E-03	2.11E-02
2nd, 80	0.1545		2.51E-02	0.3467		2.95E-02	0.5290		2.29E-02

Table 6 - Discretization error vs model uncertainty in void fraction at 3 positions II: closure correlations

	P1			P2			P3		
	Mean	DE	ME	Mean	DE	ME	Mean	DE	ME
	Saha-Zuber								
1st, 20	0.2051	5.21E-02	1.16E-02	0.3982	5.17E-02	4.81E-03	0.5574	2.78E-02	7.72E-04
1st, 40	0.1794	2.64E-02	1.23E-02	0.3743	2.79E-02	5.40E-03	0.5443	1.47E-02	9.20E-04
1st, 80	0.1657	1.27E-02	1.30E-02	0.3608	1.43E-02	5.97E-03	0.5371	7.56E-03	1.05E-03
2nd, 20	0.1556	2.57E-03	1.39E-02	0.3469	3.64E-04	6.82E-03	0.5322	2.69E-03	1.16E-03
2nd, 40	0.1542	1.13E-03	1.33E-02	0.3468	2.68E-04	6.53E-03	0.5289	6.55E-04	1.18E-03
2nd, 80	0.1530		1.40E-02	0.3465		6.80E-03	0.5296		1.13E-03
	Interfacial friction								
1st, 20	0.2060	5.31E-02	1.20E-03	0.3986	5.22E-02	1.61E-03	0.5575	2.81E-02	1.31E-03
1st, 40	0.1791	2.62E-02	1.17E-03	0.3741	2.77E-02	1.62E-03	0.5442	1.47E-02	1.39E-03
1st, 80	0.1657	1.28E-02	9.40E-04	0.3607	1.43E-02	1.56E-03	0.5370	7.60E-03	1.41E-03
2nd, 20	0.1545	1.57E-03	7.57E-04	0.3461	2.67E-04	1.56E-03	0.5319	2.48E-03	1.57E-03
2nd, 40	0.1532	2.56E-04	9.85E-04	0.3461	2.32E-04	1.59E-03	0.5286	8.13E-04	1.48E-03
2nd, 80	0.1529		9.21E-04	0.3464		1.67E-03	0.5294		1.51E-03
	Wall-to-liquid friction								
1st, 20	0.2059	5.30E-02	2.30E-04	0.3985	5.20E-02	4.23E-04	0.5574	2.79E-02	4.75E-04
1st, 40	0.1792	2.63E-02	2.00E-04	0.3742	2.78E-02	3.83E-04	0.5443	1.48E-02	4.67E-04
1st, 80	0.1657	1.28E-02	1.66E-04	0.3607	1.43E-02	3.71E-04	0.5371	7.60E-03	4.79E-04
2nd, 20	0.1545	1.63E-03	1.37E-04	0.3463	9.99E-05	3.47E-04	0.5322	2.67E-03	5.00E-04
2nd, 40	0.1532	3.31E-04	1.54E-04	0.3463	9.91E-05	3.41E-04	0.5288	6.76E-04	4.62E-04
2nd, 80	0.1529		1.47E-04	0.3464		3.58E-04	0.5295		4.67E-04
	Interface-to-liquid heat transfer coefficient								
1st, 20	0.2057	5.28E-02	1.85E-03	0.3984	5.20E-02	1.31E-03	0.5574	2.79E-02	4.33E-04
1st, 40	0.1793	2.64E-02	1.44E-03	0.3742	2.78E-02	1.28E-03	0.5443	1.48E-02	4.44E-04
1st, 80	0.1657	1.28E-02	1.45E-03	0.3607	1.43E-02	1.35E-03	0.5371	7.57E-03	4.76E-04
2nd, 20	0.1546	1.73E-03	1.42E-03	0.3464	3.06E-05	1.34E-03	0.5322	2.64E-03	4.43E-04
2nd, 40	0.1533	3.99E-04	1.20E-03	0.3464	5.67E-05	1.30E-03	0.5288	7.06E-04	4.56E-04
2nd, 80	0.1529		1.35E-03	0.3464		1.38E-03	0.5295		4.56E-04

Table 7 - Discretization error vs input uncertainty in void fraction at 3 positions III: boundary conditions

	P1			P2			P3		
	Mean	DE	ME	Mean	DE	ME	Mean	DE	ME
	Outlet pressure								
1st, 20	0.2051	5.23E-02	8.74E-03	0.3973	5.12E-02	9.78E-03	0.5565	2.73E-02	7.27E-03
1st, 40	0.1792	2.65E-02	7.86E-03	0.3743	2.82E-02	9.90E-03	0.5443	1.50E-02	7.64E-03
1st, 80	0.1656	1.28E-02	7.70E-03	0.3604	1.43E-02	1.04E-02	0.5367	7.49E-03	8.15E-03
2nd, 20	0.1552	2.37E-03	8.04E-03	0.3470	8.67E-04	1.07E-02	0.5326	3.35E-03	8.73E-03
2nd, 40	0.1536	7.82E-04	7.31E-03	0.3467	6.05E-04	1.05E-02	0.5291	7.12E-05	8.41E-03
2nd, 80	0.1528		7.73E-03	0.3461		1.10E-02	0.5292		8.73E-03
	Inlet mass flux								
1st, 20	0.2049	5.21E-02	1.07E-02	0.3970	5.10E-02	1.19E-02	0.5563	2.71E-02	9.04E-03
1st, 40	0.1793	2.65E-02	9.73E-03	0.3743	2.82E-02	1.21E-02	0.5442	1.51E-02	9.43E-03
1st, 80	0.1656	1.28E-02	9.60E-03	0.3603	1.43E-02	1.27E-02	0.5367	7.50E-03	1.01E-02
2nd, 20	0.1553	2.46E-03	9.87E-03	0.3470	9.76E-04	1.31E-02	0.5326	3.43E-03	1.07E-02
2nd, 40	0.1537	8.41E-04	9.13E-03	0.3468	6.95E-04	1.28E-02	0.5292	2.18E-05	1.03E-02
2nd, 80	0.1528		9.56E-03	0.3461		1.34E-02	0.5292		1.06E-02
	Wall heat flux								
1st, 20	0.2084	5.46E-02	1.66E-02	0.4006	5.34E-02	1.84E-02	0.5588	2.90E-02	1.41E-02
1st, 40	0.1790	2.51E-02	1.49E-02	0.3737	2.65E-02	1.87E-02	0.5436	1.38E-02	1.47E-02
1st, 80	0.1664	1.26E-02	1.49E-02	0.3611	1.40E-02	1.96E-02	0.5372	7.33E-03	1.54E-02
2nd, 20	0.1538	7.24E-06	1.48E-02	0.3449	2.20E-03	2.02E-02	0.5308	9.31E-04	1.65E-02
2nd, 40	0.1528	9.81E-04	1.41E-02	0.3453	1.81E-03	1.97E-02	0.5279	1.93E-03	1.59E-02
2nd, 80	0.1538		1.47E-02	0.3471		2.07E-02	0.5299		1.66E-02
	Inlet water temperature								
1st, 20	0.2050	5.24E-02	8.86E-03	0.3974	5.15E-02	9.08E-03	0.5566	2.76E-02	6.02E-03
1st, 40	0.1780	2.54E-02	7.79E-03	0.3728	2.69E-02	8.98E-03	0.5432	1.41E-02	6.25E-03
1st, 80	0.1659	1.33E-02	8.09E-03	0.3608	1.49E-02	9.91E-03	0.5370	7.96E-03	7.02E-03
2nd, 20	0.1551	2.55E-03	8.19E-03	0.3468	9.87E-04	9.98E-03	0.5324	3.35E-03	7.29E-03
2nd, 40	0.1533	6.91E-04	7.48E-03	0.3462	4.06E-04	9.83E-03	0.5288	2.93E-04	7.16E-03
2nd, 80	0.1526		7.73E-03	0.3458		1.01E-02	0.5291		7.26E-03

5. ACKNOWLEDGEMENT

This work is supported by the U.S. Department of Energy, under Department of Energy Idaho Operations Office Contract DE-AC07-05ID14517. Accordingly, the U.S. Government retains a nonexclusive, royalty-free license to publish or reproduce the published form of this contribution, or allow others to do so, for U.S. Government purposes. This work is also partially supported from the DOE NEUP funding under project number 16-10630.

6. REFERENCES

[1] W.L. OBERKAMPF and C.J. ROY, *Verification and Validation in Scientific Computing*, Cambridge University Press, (2010).
[2] S. LEVY, *Two-Phase Flow in Complex Systems*, John Wiley & Sons, (1999)

[3] B.E. BOYACK, "Quantifying reactor safety margins part 1: An overview of the code scaling, applicability, and uncertainty evaluation methodology," *Nuclear Engineering and Design*, 119 (1), 1-15, (1990).
[4] Idaho National Laboratory, "RELAP5-3D Code Manual Volume I: Code Structure, System Models and Solution Methods", INEEL-EXT-98-00834, Revision 4.0, June (2012).
[5] B. CHEXAL, G. LELLOUCHE, "A Full-Range Drift-Flux Correlation for Vertical Flows (Revision 1)," EPRI NP-3989-SR, Electric Power Research Institute, (1986).
[6] L. ZOU, H. ZHAO, and H. ZHANG, "Applications of high-resolution spatial discretization scheme and Jacobian–free Newton–Krylov method in two-phase flow problems," *Annals Nuclear Energy*, 83, 101–107, (2015)
[7] L. ZOU, H. ZHAO, and H. ZHANG, "Application of Jacobian–free Newton–Krylov method in implicitly solving two-fluid six-equation two-phase flow problems: Implementation, validation and benchmark," *Nuclear Engineering and Design*, 300, 268–281, (2016)
[8] O. NYLUND, et al., "Hydrodynamic and Heat Transfer Measurements on a Full- Scale Simulated 36-Rod Marviken Fuel Element with Non-uniform Radial Heat Flux Distribution," FRIGG Loop Project, FRIGG-3, (1969)
[9] G.G. BARTOLOMEI, et al., "An experimental investigation of true volumetric vapor content with subcooled boiling in tubes," *Therm. Eng.*, 29 (3), 132–135, (1982)
[10] P. SAHA and N. ZUBER, "Point of Net Vapor Generation and Vapor Void Fraction in Subcooled Boiling," Proceedings Fifth International Heat Transfer Conference, Tokyo, Japan, September 3-7, 4, pp. 175-179, (1974).
[11] H. AUGUSTO, et al., "Uncertainty and sensitivity analyses as a validation tool for BWR bundle thermal–hydraulic predictions." *Nuclear Engineering and Design,* 241, 3697-3706 (2011).
[12] G. HU and T. Kozlowski, "Inverse uncertainty quantification of TRACE physical model parameters using BFBT benchmark data." *Annals of Nuclear Energy,* 96, 197-203 (2016).
[13] X. WU, et al., "Inverse Uncertainty Quantification of TRACE Physical Model Parameters using Sparse Grid Stochastic Collocation Surrogate Models", *Nuclear Engineering and Design*, 319, 185-200 (2017).